Journal of Structural Biology 206 (2019) 49–54

Contents lists available at ScienceDirect

Journal of Structural Biology

journal homepage: www.elsevier.com/locate/yjsbi

This article is part of the Special Issue on Solid-State NMR of Biomolecular Assemblies

Spectral comparisons of mammalian cells and intact organelles by solid-state NMR☆

Sabrina H. Werby, Lynette Cegelski*

Department of Chemistry, Stanford University, Stanford, CA 94305, USA

ARTICLE INFO

Keywords:
Solid-state NMR
CPMAS
Whole cell NMR

ABSTRACT

Whole-cell protein profiling, spatial localization, and quantification of activities such as gene transcription and protein translation are possible with modern biochemical and biophysical techniques. Yet, addressing questions of overall compositional changes within a cell – capturing the relative amounts of protein and ribosomal RNA levels and lipid content simultaneously – would require extractions and purifications with caveats due to isolation yields and detection methods. A holistic view of cellular composition would aid in the study of cellular composition and function. Here, solid state NMR is used to identify ^{13}C NMR signatures for cellular organelles in HeLa cells without the use of any isotopic labeling. Comparisons are made with carbon spectra of subcellular assemblies including DNA, lipids, ribosomes, nuclei and mitochondria. Whole-cell comparisons are made with different mammalian cells lines, with red blood cells that lack nuclei and organelles, and with Gram-negative and Gram-positive bacteria. Furthermore, treatment of mammalian cells with cycloheximide, a commonly used protein synthesis inhibitor, revealed unanticipated changes consistent with a significant increase in protein glycosylation, obvious at the whole cell level. Thus, we demonstrate that solid-state NMR serves as a unique analytical tool to catalog and compare the ratios of distinct carbon types in cells and serves as a discovery tool to reveal the workings of inhibitors such as cycloheximide on whole-cell biochemistry.

1. Introduction

Prokaryotic and eukaryotic cells both house a complex suite of macromolecular machines and biomolecules, including proteins, lipids and nucleic acids, to carry out required functions to survive, divide and respond to changing conditions. At the most fundamental level, eukaryotic cells are distinct from prokaryotic cells in their subcellular compartmentalization and use of membrane bound organelles. These organelles include the nucleus (chromosomal DNA storage), the mitochondrion (ATP/energy generation), the Golgi (protein processing) and the Endoplasmic Reticulum (protein processing, sorting, and transport). Molecules are targeted to and transported through these organelles, often undergoing transformations along the way, eliciting visions of a bustling city. Misfunction of any cellular organelle can wreak havoc and result in aberrant biochemistry and disease. Enormous effort has been dedicated to understanding each organelle in as complete detail as possible and in understanding how each organelle interfaces with the rest of the cell. Recently, full 3D structures of mitochondria and nuclei have even been determined using Coherent X-ray Diffractive Imaging (CXDI) (Kim et al., 2017; Song et al., 2014). Protein assemblies within these organelles have been elucidated using cryo-EM (Bausewein et al., 2017; Chua and Sandin, 2017; D'Imprima et al., 2016; Mahamid et al., 2016; Wilson and Costa, 2017; Zhou et al., 2015).

Impressive advances in structural biology methods, including X-ray crystallography, cryo-EM, solution and solid-state NMR, continue to transform our understanding of larger and larger assemblies. Information regarding dynamics of proteins and macromolecular assemblies in the relevant milieu of the cell is also advancing our knowledge beyond static structures. Yet, quantifying composition and concentrations of biomolecules in cells is usually the target of specific biochemical experiments. Western blot immunoassays, for example, can quantitatively compare the relative amount of a particular protein present across a sample set. Two-dimensional protein gel analysis and proteomics approaches can also be used to evaluate changes across all proteins in a cell, and qRTPCR or RNA-Seq can be employed to evaluate the prevalence of mRNA (and other RNAs), indicative of gene expression status. However, readily and quickly identifying collective differences in overall composition, such as quantifying the relative abundance of proteins, nucleic acids, carbohydrates and lipids, between samples poses a challenge to typical biochemical analyses. These usually rely on complete liberation and solubilization of all these components, followed by

☆ This Special Issue is edited by Tatyana Polenova, Amir Goldbourt, and Guido Pintacuda, and highlights the state of the art in structural biology of biomolecular assemblies by solid-state NMR.

* Corresponding author.
E-mail address: cegelski@stanford.edu (L. Cegelski).

https://doi.org/10.1016/j.jsb.2018.05.007
Received 6 December 2017; Received in revised form 15 March 2018; Accepted 25 May 2018
Available online 30 May 2018
1047-8477/

specific biochemical assays.

Solid-state NMR has emerged as a powerful tool to monitor atomic-level compositional changes in large cellular assemblies and in whole cells. We have worked extensively with bacterial cell walls and whole cells and have identified and developed spectral signatures of specific cell wall atoms and bonds with a variety of approaches utilizing spin-1/2 nuclei, primarily through ^{13}C and ^{15}N detection, REDOR measurements, and spin diffusion (reviewed in Romaniuk and Cegelski, 2015). Selective labeling has been invaluable in identifying specific D-Ala-Gly crosslinks, for example, in *S. aureus* isotopically labeled with the two amino acids through their supplementation in the nutrient growth medium (Cegelski et al., 2002; Kim et al., 2008). Formation of D-Ala-Gly crosslinks is inhibited by penicillin and solid-state NMR enables the direct measurement of the extent of diminution of crosslink formation in whole cell samples. Uniform labeling with ^{13}C has been recruited for spin diffusion measurements in cell walls and whole cells (Nygaard et al., 2015). Compositional detail is also obtained from examining samples with ^{13}C at natural abundance. The first determinations of the composition of the extracellular matrix surrounding biofilm bacteria in uropathogenic *E. coli* were made using bacterial samples with natural abundance ^{13}C levels (McCrate et al. 2013; Thongsomboon et al., 2018). In studies with *S. aureus*, spectral signatures for cell walls have been identified in unlabeled whole cells. Moreover, this approach had the sensitivity to distinguish cells as being treated with the antibiotic fosfomycin (a cell-wall inhibitor) and chloramphenicol (a protein synthesis inhibitor) (Nygaard et al., 2015). More recently, we reported the ^{13}C CPMAS spectrum of intact bacterial ribosomes, which can account for up to one-fourth of the cell mass (Nygaard et al., 2017).

Here, we present the ^{13}C CPMAS spectra of nuclei and mitochondria isolated from eukaryotic HeLa cells and identify spectroscopic signatures of these organelles in a HeLa whole-cell spectrum. Nuclei and mitochondria exhibit distinct regions of spectral enhancement and diminution that correspond to the unique contributions and density of carbon types present within them. We further compared these spectral signatures in HeLa cells with red blood cells and bacterial cells. Finally, our results with a commonly employed protein synthesis inhibitor, cycloheximide, revealed new insights regarding the extent of its additional effect on protein glycosylation in whole cells. All samples were analyzed at natural abundance ^{13}C levels, with no isotopic enrichment. Thus, this approach is applicable to analyzing more complex cell types and tissue specimens where biosynthetic labeling is not always feasible.

2. Materials and methods

2.1. Solid-state NMR measurements

All NMR experiments were performed in an 89 mm bore 11.7 T magnet (Agilent Technologies, Danbury, CT) using an HCN Agilent probe with a DD2 console (Agilent Technologies). Samples were spun at 7143 Hz in 36 μL capacity 3.2 mm rotors. The temperature was maintained at 5 °C with an FTS chiller (FTS Thermal Products, SP Scientific, Warminster, PA) supplying nitrogen at -10 °C. The field strength for ^{13}C cross polarization was 50 kHz with a 10% ^{1}H linear ramp centered at 57 kHz. The CPMAS recycle time was 2 s for all experiments. ^{13}C chemical shifts were referenced to tetramethylsilane as 0 ppm using a solid adamantine sample at 38.5 ppm.

2.2. Bacterial cell culturing

Whole cell samples of the *E. coli* strain MC4100 and the *S. auerus* strain ATCC29213 were grown, frozen and lyophilized for NMR analysis. Specifically, a bacterial culture was initiated in LB broth (*E. coli*) or *S. aureus* synthetic medium (SASM – a specialized media for growing *S. auerus)* and grown overnight and then diluted 1:500 in LB broth (*E. coli*) or 1:300 in SASM (*S. aureus*). Bacteria were grown shaking at 37 °C until mid-exponential phase. *E. coli* cells were then harvested by centrifugation at 5000 *g* for 15 min and washed twice with cold borate buffered saline. *S. aureus* cells were harvested by centrifugation at 10,000 *g* for 10 min and washed three times with ice cold 5 mM Hepes buffer (pH 7). All whole cell pellets were frozen in liquid nitrogen and lyophilized.

2.3. Cell culture and organelle isolations

HeLa and HEK cells were grown in Dulbecco's Modified Eagle Medium (DMEM) while CHO cells were grown in Ham's F-12 K (Kaighn's) Medium. All media was supplemented with 10% fetal bovine serum (FBS) and 1% (v/v) penicillin–streptomycin. Cells were grown until confluent at 37 °C and 5% CO_2. Mammalian cells were harvested by trypsinizing and then spun at 1200 *g* for 10 min at 4 °C. Cells were then washed in cold borate buffered saline. For whole cell samples, these cell pellets were frozen in liquid nitrogen and lyophilized. From this stage, mitochondria and nuclei were extracted from HeLa cells by differential centrifugation as previously described with modifications (Clayton and Shadel, 2014; Nilsen, 2013). Specifically, cells were re-suspended in five times the pellet cell volume of hypotonic lysis buffer (1.5 mM $MgCl_2$, 10 mM KCl, 1% (v/v) borate buffered saline in MilliQ water). Cells were then left on ice for 15 min to swell and were lysed by use of a dounce homogenizer (pestle B) until greater than 90% cell lysis was achieved (~14 strokes). The lysate was then spun for 10 min at 600 *g* at 4 °C for 10 min to pellet intact nuclei. The supernatant from this step was spun again at 8000 *g* at 4 °C for 10 min to pellet intact mitochondria. Both the nuclei and the mitochondria pellets were washed in cold borate buffered saline twice. The mitochondria and nuclei pellets were frozen in liquid nitrogen and lyophilized.

2.4. Red blood cell isolation

Red blood cells were isolated from human blood (Innovative Research Inc) by centrifugation. The blood was spun down at 1000 *g* for 10 min × 4 °C. The pellet was resuspended in borate buffered saline and spun again under the same conditions as above. This process was repeated until the supernatant was clear while the pellet was bright red. The cell pellet was frozen in liquid nitrogen and lyophilized.

2.5. DNA preparation

DNA (Deoxyribonucleic acid sodium salt from *E. coli* Strain B) was commercially acquired (Sigma Aldrich) and used as received (dry powder).

2.6. Cycloheximide treatment

HeLa cells were treated with a non-lethal concentration of cycloheximide as previously described (Adams and Cooper, 2007; Oksvold et al., 2012). HeLa cells were grown under the conditions described above for 16 h at which point the media was replaced with media containing 50 μg/mL cycloheximide. The cells were grown for another 8 h before harvesting.

2.7. Organelle fluorescence labeling for confocal microscopy

8.75×10^5 HeLa cells were seeded onto #1 ½ square coverslips and grown overnight. The cells were fixed and permeabilized as previously described with modifications (Chazotte, 2011). Cells were rinsed three times with PBS and then fixed for 10 min in 3.7% formaldehyde. The cells were then washed with PBS for five minutes three times. Mitochondria were then stained with MitoTracker Deep Red 633 according to manufacturer's instructions with modifications. Cells were incubated in he MitoTracker probe (25 nM in PBS) for 20 min. The cells were then permeabilized in 0.2% Triton X-100 for 5 min and then washed three times with PBS. The ribosomes were then immunostained

according to manufacturer's instructions with modifications. The cells were blocked for 1 h at room temperature in blocking buffer (1% bovine serum albumin) spiked with 0.2% Triton X-100. Cells were then incubated for 45 min in blocking buffer containing a 1:25 dilution of primary antibody (anti-ribosomal protein S3) and then washed three times with PBS. The cells were then incubated for 30 min in blocking buffer containing a 1:500 dilution of secondary antibody (Alexa-Fluor 488 goat anti rabbit) and then rinsed three times with PBS. The nuclei were then stained with a DAPI solution (0.2 μg/mL) for one minute and rinsed with PBS three times. The tri-stained coverslips were then mounted onto slides and imaged using a Zeiss 880 inverted confocal system.

3. Results and discussion

3.1. Carbon compositional comparisons of intact mammalian cells and isolated organelles

Three commonly used mammalian cell lines were selected for comparative analysis by CPMAS solid-state NMR. These include HeLa cells (human cervical cancer cell line), Human Embryonic Kidney cells (HEK), and Chinese Hamster Ovarian cells (CHO). All ^{13}C detection experiments in this work are performed without isotopic labeling, with ^{13}C at natural abundance levels. The ^{13}C CPMAS spectra of the three mammalian cell lines are extremely similar and display strong overlap in all regions (Fig. 1A). The types of carbons contributing to the spectra can be identified and categorized. Each whole cell spectrum contains a prominent carbonyl region (172 ppm), a region associated with sp_2 carbons as in nucleic acids and aromatic amino acids (130–160 ppm), a region associated with alcohol and sugar carbons (70–85 ppm), amino acid alpha carbons (40–60 ppm), and the upfield aliphatic peaks including methyls and lipid CH_2 groups (10–40 ppm), etc. A single whole cell spectrum with all the contributions of carbonyls contributing broadly to a certain region and carbohydrates to others, etc., might not appear to ultimately be that specific or capable of addressing specific biological questions. In the following sections, we aim to show how there is power in observing the carbon pools in this way for intact cellular systems and in making spectral comparisons across samples. We also find that solid-state NMR analysis of these types of intact systems is also serving as a discovery tool to reveal unanticipated compositional details and we provide an example of this with the whole cell NMR analysis of mammalian HeLa cells treated with cycloheximide, typically employed for its ability to interrupt protein synthesis.

Each of the three mammalian whole cell spectra in Fig. 1A represents the collection of all the carbons in the cells, including those from within membrane-bound organelles. Each cell has a nucleus housing the cellular DNA, totaling 6–8% of the cell volume (Jorgensen et al., 2007). Mitochondria are the sites of ATP synthesis, fueling the energy demands of the cell and are spread throughout the cytoplasm, encompassing as much as 35% of the cellular mass (Anastacio et al. 2013). Nuclei and mitochondria are readily isolated from HeLa cells by differential centrifugation and were examined by ^{13}C CPMAS NMR (Fig. 1B-C). Fluorescence microscopy of these HeLa cells illustrates the localization of nuclei (blue) and mitochondria (red). Ribosomes are also identified in green. Ribosomes are not membrane-bound structures, but are the cellular machines that carry out protein synthesis. We recently reported the ^{13}C and ^{15}N CPMAS spectra of intact ribosomes isolated from *E. coli* (Nygaard et al., 2017). Ribosomes naturally exhibit dramatic differences from whole cells and other cellular assemblies, based on their unique protein-RNA composition and the defining ^{13}C chemical shifts for nucleic acid carbons. Here, we begin the analysis of mammalian cell NMR signatures by presenting the ^{13}C spectra of isolated nuclei and mitochondria in comparison with the intact HeLa cells (Fig. 1B & C).

The nucleus is the largest cellular organelle and, overall, has a similar ^{13}C CPMAS spectrum to that of whole cells (Fig. 1B). Key differences are the increases in peak intensity for the DNA purine and pyrimidine carbons between 130 and 160 ppm and the C1′, C3′, and C4′ deoxyribose carbons near 85 ppm. A comparative spectrum of isolated DNA is also provided (green inset). Whole cells also contain ribosomes that contribute intensity to these regions due to the significant ribosomal RNA content. Yet, along with all the nuclear proteins, nuclei contain a higher density of DNA than the ribosomal RNA density found

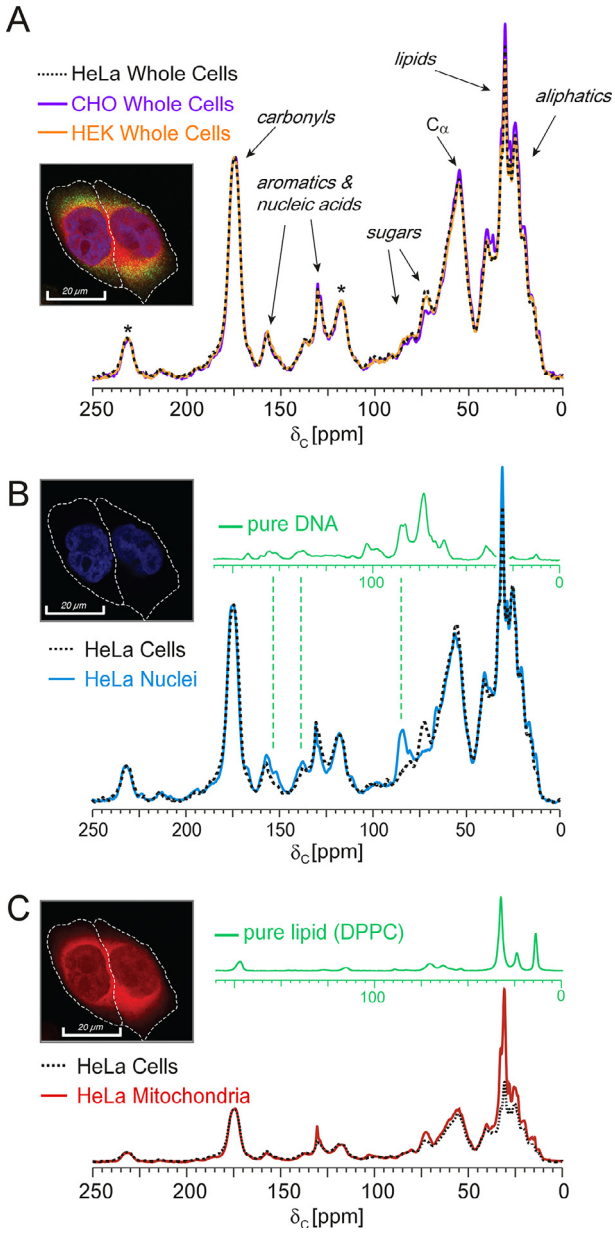

Fig. 1. Mammalian whole cells and organelles by ^{13}C NMR. All spectra were normalized to the carbonyl peak height at 176 ppm to enable the most facile comparisons and contrasts. (A) ^{13}C CPMAS spectral overlays of whole HEK, HeLa, and CHO cells reveal highly similar ^{13}C spectra for three mammalian cell lines. General types of carbon contributions are annotated and spinning sidebands are represented by asterisks. Image inset: confocal microscopy image of a dividing HeLa cell with nuclei (blue), mitochondria (red), and ribosomes (green) labeled. (B) ^{13}C CPMAS spectral overlay of whole HeLa cells and nuclei isolated from HeLa cells. Image inset: Confocal microscopy image of a dividing HeLa cell with nuclei labeled with DAPI. Spectral inset: ^{13}C CPMAS spectrum of pure DNA. (C) ^{13}C CPMAS spectral overlay of whole HeLa cells and mitochondria isolated from HeLa cells. Image inset: Confocal microscopy image of a dividing HeLa cell with mitochondria labeled with MitoTracker Deep Red 633. Spectral inset: ^{13}C CPMAS spectrum of DPPC phospholipids.

in whole cells and this is reflected in the relative enhancement in the DNA-specific ^{13}C spectral regions for nuclei. As seen from the pure DNA spectrum, DNA also contributes peak intensity near 73 ppm. This is the dominant peak observed in pure DNA. Yet, many other hydroxyl carbons in the whole cell also share this chemical shift. Since this peak is decreased in the nucleus spectrum relative to the whole-cell comparison, it indicates that other C-OH carbons at this chemical shift are relatively more prevalent by carbon mass in whole cells than in nuclei. The lipid peak at 30 ppm is more intense in the nucleus spectrum compared to the whole cell spectrum. This could be attributed to the smaller volume of a nucleus compared to a whole cell (and an increased surface area to volume ratio), causing the phospholipid carbons to proportionally make up more of the overall carbon mass of nuclei than in whole cells.

Mitochondria are responsible for cellular energy production and tend to cluster in areas where energy is most needed, e.g. at sites of cell division (Fig. 1C inset). The ^{13}C CPMAS spectrum of isolated mitochondria, with their resident biomolecular components, reveals that mitochondria share the same general carbon pools as whole cells (Fig. 1C). However, mitochondria exhibit dramatic enhancements in lipid-associated peak intensities (25–40 ppm). This enhancement is even more pronounced than for nuclei vs whole cells and is attributed to the even greater increase in surface area to volume ratio for mitochondria, wherein mitochondria consist of a vast membranous ruffling architecture to enhance surface area.

3.2. Red blood cells as unique cells that lack nuclei and membrane-bound organelles

Red blood cells are an amazing cell type that, in their mature form, consist of approximately 97% hemoglobin and account for roughly one-fourth of the cells in the human body (Weed et al., 1963). During their development, red blood cells ramp up ribosome production to make hemoglobin and ultimately eject their nucleus to become specialized carriers of hemoglobin, picking up oxygen in the lungs and delivering it to tissues via the circulatory system. Red bloods cells also lack mitochondria. The absence of nuclei and other organelles contributes to the concave disk shape of red blood cells. We compared isolated red blood cells from human blood to HeLa whole cells and to pure hemoglobin by ^{13}C CPMAS NMR (Fig. 2A). The red blood cell spectrum is a very close match to pure hemoglobin (Fig. 2B). Even without the direct hemoglobin comparison, it is obvious that the red blood cell spectrum lacks the nucleic acids that contribute to the HeLa whole cell spectrum, with purines and pyrimidines notably present in HeLa cells from 130 to 160 ppm and deoxyribose peaks near near 85 ppm (Fig. 2C).

3.3. Whole cell NMR comparison of mammalian and bacterial cells

The ^{13}C CPMAS spectrum of HeLa cells was compared with both Gram-negative and Gram-positive bacterial cells (Fig. 3). We hypothesized that mammalian cells would compositionally be more similar to Gram-negatives than to Gram-positives, primarily because Gram-positive bacteria surround themselves with a thick cell wall that can account for 15–25% of the cell mass and is composed of compositionally unique biomolecules: peptidoglycan and teichoic acids, both very rich in polysaccharide content. Gram-negative bacteria, on the other hand, are rod shaped organisms and contain inner and outer membranes that surround the cytoplasmic contents, including ribosomes, DNA, proteins, etc. The periplasm is the space between the two membranes and contains only a thin layer of peptidoglycan plus many proteins. We also note that the bacterial outer membrane composition is distinct from the inner membrane and is rich in lipopolysaccharides. ^{13}C CPMAS spectra of HeLa cells and *E. coli* exhibited significant similarities in the general peak positions, shapes, and heights (Fig. 3A). The *E. coli* whole cell spectrum, however, is enhanced in the peaks between 35 and 40 ppm, 60–100 ppm and 135–160 ppm in the comparison as normalized to the carbonyls peaks. These peaks correspond to the major carbon signatures present in *E. coli* ribosomes (Nygaard et al. 2017) and are consistent with the increased percentage of the cell volume occupied by ribosomes in *E. coli*, lacking other organelles, as compared to HeLa cells. In contrast, the peaks at 130 ppm and 30 ppm are enriched in the HeLa cell when compared with the *E. coli* spectrum, and these peaks were notably enhanced in the isolated mitochondria spectrum. Thus, the spectral differences between HeLa cells and *E. coli* can be rationalized based on the compositional differences of major subcellular components emphasized in Fig. 2.

As hypothesized, the ^{13}C CPMAS spectrum of *S. aureus*, a Gram-positive bacterium, exhibited considerable differences in relative carbon composition as compared with HeLa cells. We attribute this to the dominant contributions of cell-wall carbons to the *S. aureus* spectrum, resulting in the relatively lower signal intensities for intracellular components (distinguished in contributions to the 125–160 ppm region not populated by cell-wall carbons) and increased cell wall carbons, notably represented by the cell wall polysaccharide anomeric carbons and other sugar ring carbons, collectively between 65 and 105 ppm (Nygaard et al. 2015). Thus, whole cell spectra have the ability to report on the total collection of carbons in the cell and, through comparison with standard cell types and major molecular assemblies, can be interpreted in terms of major types of biomolecules in different cell types. We additionally sought to further test the power of the whole cell NMR approach with mammalian cells to see whether the resulting spectrum for cells treated with a protein synthesis inhibitor would lead to detectable changes in the whole cell spectrum, with suppression of protein-specific signals.

3.4. Cycloheximide treated HeLa cells

As described earlier, we determined that ^{13}C CPMAS of natural abundance *S. aureus* could reveal the general nature of inhibition

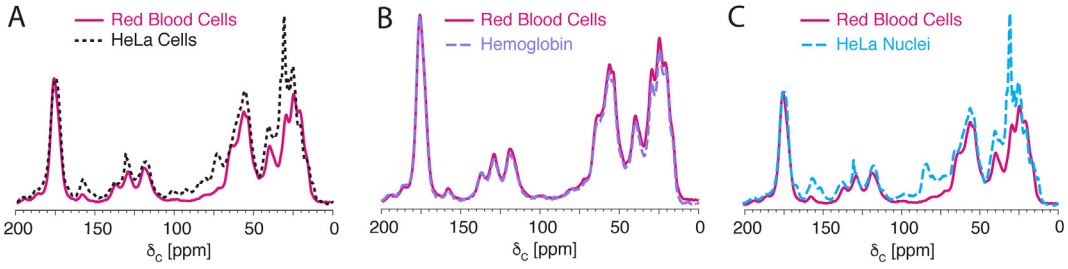

Fig. 2. Examination of red blood cells by ^{13}C NMR. (A) A spectral overlay of red blood cells (solid red line) with HeLa cells (dashed black) reveals significant carbon differences, with reduced contributions from DNA and ribosomes to the red blood cell spectrum. (B) The red blood cell ^{13}C spectrum is a close match to that of hemoglobin, wherein red blood cells are composed of at least 85% hemoglobin by mass. (B) A spectral overlay of whole red blood cells with nuclei isolated from HeLa cells further emphasizes the lack of contributions from nucleic acids to the red blood cell spectrum, similar to the differences observed in the comparison of red blood cells with whole HeLa cells in (A).

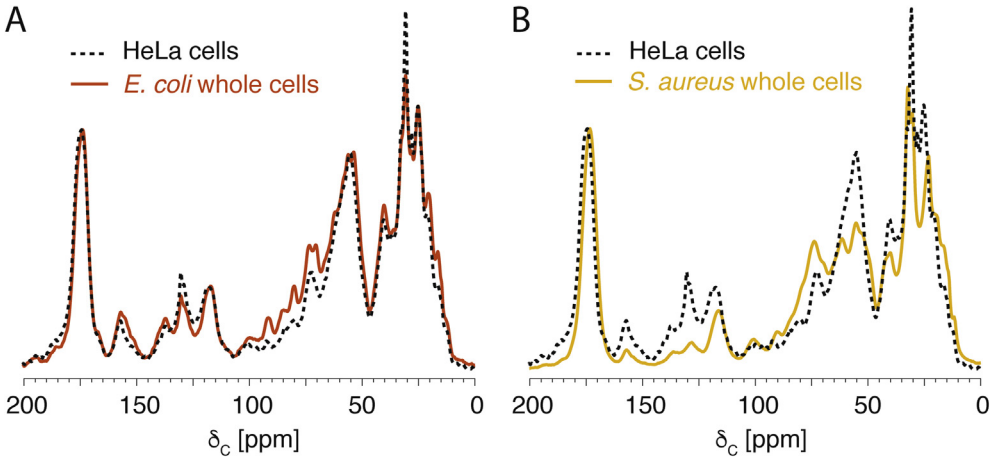

Fig. 3. ^{13}C NMR comparison of HeLa cells with Gram-negative and Gram-positive bacteria. (A) ^{13}C CPMAS spectra of HeLa whole cells and *E. coli* (Gram-negative bacterium) whole cells exhibit major overall similarities, yet the *E. coli* spectrum exhibits enhanced signal intensity between 65 and 105 ppm, while the HeLa spectrum is enhanced at 130 ppm and 30 ppm, as peaks associated with lipids. (B) ^{13}C CPMAS spectral overlay of HeLa whole cells and *S. aureus* (Gram-positive bacterium) whole cells reveals very different spectral signatures due to the presence of a thick, peptidoglycan-rich cell wall in Gram-positive bacteria.

among antibiotics, detecting reduced cell wall content for cell-wall targeting antibiotics, for example (Nygaard et al. 2015). Here, HeLa cells were treated with cycloheximide, a known inhibitor of protein synthesis widely used in biochemical experiments. A concentration of drug was used that is not so high a concentration as to effect immediate cell killing, avoiding massive cell lysis. Treatment of HeLa cells with a 50 μg/mL concentration of cycloheximide reduced cell viability by only 5–10% after an 8-h treatment.

The ^{13}C CPMAS spectrum of cycloheximide-treated HeLa cells was compared to the control HeLa cell spectrum (Fig. 4). Instead of observing relative differences in protein-associated peaks, the very obvious difference between the two spectra was the enhancement of carbons associated with closed ring sugars as found for mannosylated and other glycosylated proteins. Cycloheximide is know to bind to the 60S subunit of the eukaryotic ribosome to inhibit translation, yet its exact mechanism of action is appreciated to be incompletely understood (Schneider-Poetsch et al., 2010) and other effects have been documented. Indeed, an enhancement on protein glycosylation has been observed previously. A biotechnology application involving the production of recombinant human protein prolactin recruited the use of cycloheximide because the N-linked glycosylation site occupancy of the protein was increased during treatment (Shelikoff et al., 1994). More specifically, prolactin has 199 amino acids, one of which is an asparagine and a target for N-linked glycosylation. Only about 15–30% of prolactin produced in different cell types is glycosylated. In contrast to other protein synthesis inhibitors studied, cycloheximide uniquely resulted in enhanced glycosylation of prolactin. The authors provided an attractive model for this activity and suggested that the decreased rate of elongation during translation could decrease the rate at which nascent polypeptides enter and are processed in the endoplasmic reticulum (ER), leading to increased residence time in the ER and an increased propensity to be a target for glycosylation (Shelikoff et al., 1994). Prolactin was studied and detected by Western blot assays using specific antibodies and more general protein profiling was not performed. Our NMR results demonstrate that glycosylation is significantly enhanced at the level of the whole proteome by simply observing the natural abundance ^{13}C spectrum of control and cycloheximide-treated whole-cell samples.

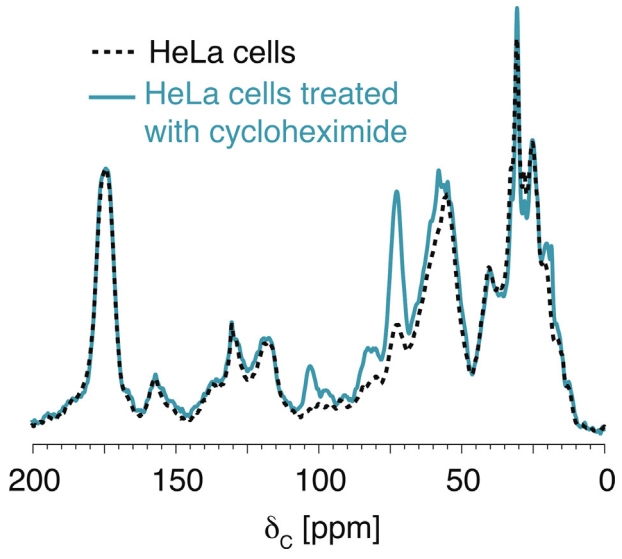

Fig. 4. Cycloheximide treatment of HeLa cells. ^{13}C spectral comparison of untreated HeLa cells and HeLa cells treated with 50 μg/mL cycloheximide for 7.5 h reveals enhanced intensity between 55 and 105 ppm, consistent with cycloheximide resulting in a significant increase in glycosylation of proteins in the whole cell sample.

4. Conclusions

Solid-state NMR has a long and rich history in examining composition and architecture in biomolecular assemblies and also in non-biological materials. We have been pursuing efforts to define parameters of cellular composition that could be used to evaluate challenging biochemical questions. Most of our work has been focused on microorganisms and some examinations of plants. In this work, we demonstrate the ability to interpret NMR spectra from mammalian whole cells. This foundation sets the stage for identifying compositional changes associated with cellular misfunction and disease. For example, the nucleus contains two main structures: the nuclear envelope and the nuclear matrix. Deviations from normal nuclear matrix composition have been implicated in cell abnormalities with severe disease phenotypes, including premature aging diseases (Cau et al., 2014). Mitochondrial compositional changes have been associated with human disease. Alterations in the phospholipid composition of synaptic mitochondrial membranes have also been shown to accompany early stages of Alzheimer's disease (Monteiro-Cardoso et al., 2015). An ability to measure parameters of composition and to provide holistic and quantitative comparisons among samples is an attractive approach to guide analysis of biochemical changes in a cell or tissue. All the experiments in this study were performed with cells and assemblies containing ^{13}C at natural abundance levels with no isotopic labeling or special growth requirements. Thus, it is possible to examine isolated mitochondria from animals and human samples to determine if the approach will be sensitive enough to detect compositional changes that lead to mitochondrial diseases, for example.

The whole-cell NMR approach shows particular promise in characterizing the modes of action of drugs and compounds whose activities

are incompletely or poorly understood. We demonstrated this and the ability of the solid-state NMR approach to serve as such a discovery tool by reporting spectroscopic changes that occur when cells are treated with cycloheximide, a commonly employed protein synthesis inhibitor. The specific spectral increases in the sugar carbons are most consistent with a major increase in protein glycosylation in whole cells. This was not anticipated, but provides insight into the effects of cycloheximide treatment, so widely used in cell biology and biochemistry experiments. Thus, researchers employing cycloheximide as a routine tool for suppressing protein synthesis should be aware of the magnitude of the effect on protein glycosylation and consider this as a possible contributor to altered outcomes in comparative experiments. This specific example is supported by individual literature examples that point to surprising aspects of cycloheximide treatment. This also emphasizes the need to consider multiple targets and activities of small molecules, even when a primary mode of action is ascribed to a compound. We believe that the holistic whole cell NMR approach is a straightforward analysis that provides value in examining gross changes in composition as a function of compound treatment or alternate environmental stresses, complementing biochemical analyses. For further carbon-type and molecular specificity, other NMR experiments could be added to more selectively filter carbon types spectroscopically and even map proximities between drugs and cellular targets as we and others have demonstrated extensively in bacteria (Cegelski et al. 2006; Cegelski, 2013). Future work will examine the influence of other small molecule effectors targeting different aspects of mammalian biochemistry to further test this approach and potentially yield unanticipated insights as we observed with our first test compound cycloheximide.

Acknowledgements

L.C. acknowledges support from the National Science Foundation CAREER Award (No. 1453247) and the National Institute of General Medical Sciences of the National Institutes of Health (R01GM117278).

References

Adams, K.W., Cooper, G.M., 2007. Rapid turnover of Mcl-1 couples translation to cell survival and apoptosis. J. Biol. Chem. 282, 6192–6200. http://dx.doi.org/10.1074/jbc.M610643200.

Anastacio, M.M., Kanter, E.M., Makepeace, C., Keith, A.D., Zhang, H., Schuessler, R.B., Nichols, C.G., Lawton, J.S., 2013. The relationship between mitochondrial matrix volume and cellular volume in response to stress and the role of the adenosine triphosphate sensitive potassium channel. Circulation 128, S130–S135. http://dx.doi.org/10.1161/CIRCULATIONAHA.112.000128.

Bausewein, T., Mills, D.J., Langer, J.D., Nitschke, B., Nussberger, S., Kühlbrandt, W., 2017. Cryo-EM structure of the TOM core complex from neurospora crassa. Cell 170 (693–700), e7. http://dx.doi.org/10.1016/j.cell.2017.07.012.

Cau, P., Navarro, C., Harhouri, K., Roll, P., Sigaudy, S., Kaspi, E., Perrin, S., De Sandre-Giovannoli, A., Lévy, N., 2014. Nuclear matrix, nuclear envelope and premature aging syndromes in a translational research perspective. Semin. Cell Dev. Biol. Regul. Spermatogenesis Nucl. Envelope Proteins Health Diseases 29, 125–147. http://dx.doi.org/10.1016/j.semcdb.2014.03.021.

Cegelski, L., Hing, A.W., Kim, S.J., Studelska, D.R., O'Connor, R.D., Mehta, A.K., Schaefer, J., 2002. REDOR characterization of vancomycin mode of action in *S. aureus*. Biochemistry 41, 13053–13058.

Cegelski, L., Steuber, D., Mehta, A.K., Kulp, D.W., Axelsen, P.H., Schaefer, J., 2006. Conformational and Quantitative Characterization of Oritavancin-Peptidoglycan Complexes in Whole Cells of *Staphylococcus aureus* by *in vivo* ^{13}C and ^{15}N Labeling. Journal of Molecular Biology 357, 1253–1262.

Cegelski, L., 2013. REDOR NMR for drug discovery. Bioorg. Med. Chem. Lett. 23, 5767–5775.

Chazotte, B., 2011. Labeling Nuclear DNA Using DAPI. Cold Spring Harb. Protoc. 2011, pdb.prot5556. https://doi.org/10.1101/pdb.prot5556.

Chua, E.Y.D., Sandin, S., 2017. Advances in phase plate cryo-EM imaging of DNA and nucleosomes. Nucleus 8, 275–278. http://dx.doi.org/10.1080/19491034.2017.1287643.

Clayton, D.A., Shadel, G.S., 2014. Isolation of Mitochondria from Tissue Culture Cells. Cold Spring Harb. Protoc. 2014, pdb.prot080002. https://doi.org/10.1101/pdb.prot080002.

D'Imprima, E., Mills, D.J., Parey, K., Brandt, U., Kühlbrandt, W., Zickermann, V., Vonck, J., 2016. Cryo-EM structure of respiratory complex I reveals a link to mitochondrial sulfur metabolism. Biochim. Biophys. Acta BBA - Bioenerg. 1857, 1935–1942. http://dx.doi.org/10.1016/j.bbabio.2016.09.014.

Jorgensen, P., Edgington, N.P., Schneider, B.L., Rupes, I., Tyers, M., Futcher, B., 2007. The size of the nucleus increases as yeast cells grow. Mol. Biol. Cell 18, 3523–3532 https://doi.org/1091/mbc.E06-10-0973.

Kim, S.J., Cegelski, L., Stueber, D., Singh, M., Dietrich, E., Tanaka, K.S., Parr, T.R., Farand, A.R., Schaefer, J., 2008. Oritavancin exhibits dual mode of action to inhibit *s. aureus* peptidoglycan biosynthesis. J. Mol. Biol. 377, 281–293.

Kim, Y., Kim, C., Kwon, O.Y., Nam, D., Kim, S.S., Park, J.H., Kim, S., Gallagher-Jones, M., Kohmura, Y., Ishikawa, T., Song, C., Tae, G., Noh, D.Y., 2017. Visualization of a mammalian mitochondrion by coherent X-ray diffractive imaging. Sci. Rep. 7. http://dx.doi.org/10.1038/s41598-017-01833-x.

Mahamid, J., Pfeffer, S., Schaffer, M., Villa, E., Danev, R., Cuellar, L.K., Förster, F., Hyman, A.A., Plitzko, J.M., Baumeister, W., 2016. Visualizing the molecular sociology at the HeLa cell nuclear periphery. Science 351, 969–972. http://dx.doi.org/10.1126/science.aad8857.

McCrate, O.A., Zhou, X., Reichhardt, C.C.R., Cegelski, L., 2013. Sum of the parts: composition and architecture of the bacterial extracellular matrix. J. Mol. Biol. 425, 4286–4294.

Monteiro-Cardoso, V.F., Oliveira, M.M., Melo, T., Domingues, M.R.M., Moreira, P.I., Ferreiro, E., Peixoto, F., Videira, R.A., 2015. Cardiolipin profile changes are associated to the early synaptic mitochondrial dysfunction in alzheimer's disease. J. Alzheimers Dis. 43, 1375–1392. http://dx.doi.org/10.3233/JAD-141002.

Nilsen, T.W., 2013. Preparation of Nuclear Extracts from HeLa Cells. Cold Spring Harb. Protoc. 2013, pdb.prot075176. https://doi.org/10.1101/pdb.prot075176.

Nygaard, R., Romaniuk, J.A.H., Rice, D.M., Cegelski, L., 2017. Whole ribosome NMR: dipolar couplings and contributions to whole cells. J. Phys. Chem. B 121, 9331–9335. http://dx.doi.org/10.1021/acs.jpcb.7b06736.

Nygaard, R., Romaniuk, J.A.H., Rice, D.M., Cegelski, L., 2015. Spectral snapshots of bacterial cell-wall composition and the influence of antibiotics by whole-cell NMR. Biophys. J. 108, 1380–1389. http://dx.doi.org/10.1016/j.bpj.2015.01.037.

Oksvold, M.P., Pedersen, N.M., Forfang, L., Smeland, E.B., 2012. Effect of cycloheximide on epidermal growth factor receptor trafficking and signaling. FEBS Lett. 586, 3575–3581. http://dx.doi.org/10.1016/j.febslet.2012.08.022.

Romaniuk, J.A.H., Cegelski, L., 2015. Bacterial cell wall composition and the influence of antibiotics by cell-wall and whole-cell NMR. Philos. Trans. R. Soc. 370, 20150024.

Schneider-Poetsch, T., Ju, J., Eyler, D.E., Dang, Y., Bhat, S., Merrick, W.C., Green, R., Shen, B., Liu, J.O., 2010. Inhibition of eukaryotic translation elongation by cycloheximide and lactimidomycin. Nat. Chem. Biol. 6 (3), 209–217. http://dx.doi.org/10.1038/nchembio.304.

Shelikoff, M., Sinskey, A.J., Stephanopoulos, G., 1994. The effect of protein synthesis inhibitors on the glycosylation site occupancy of recombinant human prolactin. Cytotechnology 15, 195–208.

Song, C., Takagi, M., Park, J., Xu, R., Gallagher-Jones, M., Imamoto, N., Ishikawa, T., 2014. Analytic 3D imaging of mammalian nucleus at nanoscale using coherent X-rays and optical fluorescence microscopy. Biophys. J. 107, 1074–1081. http://dx.doi.org/10.1016/j.bpj.2014.07.028.

Thongsomboon, W., Serra, D.O., Possling, A., Hadjineophytou, C., Hengge, R., Cegelski, L., 2018. Phosphoethanolamine cellulose: a naturally produced chemically modified cellulose. Science 359, 334–338.

Weed, R.I., Reed, C.F., Berg, G., 1963. Is hemoglobin an essential structural component of human erythrocyte membranes? J Clin Invest 42, 581–588.

Wilson, M.D., Costa, A., 2017. Cryo-electron microscopy of chromatin biology. Acta Crystallogr. Sect. Struct. Biol. 73, 541–548. http://dx.doi.org/10.1107/S2059798317004430.

Zhou, A., Rohou, A., Schep, D.G., Bason, J.V., Montgomery, M.G., Walker, J.E., Grigorieff, N., Rubinstein, J.L., 2015. Structure and conformational states of the bovine mitochondrial ATP synthase by cryo-EM. eLife 4http://dx.doi.org/10.7554/eLife.10180. e10180.